Microstructure Control and Correlation to Formability of Low Alloy Steel Via Flash Processing

Benjamin Shassere[1,†], Sudarsanam Suresh Babu[2], Gary Cola[3], Thomas Muth[1], Thomas Watkins[1]

[1]Materials Science and Technology Division, Oak Ridge National Laboratory, Oak Ridge, TN 37831, USA
[2]Department of Mechanical, Aerospace, and Biomedical Engineering, The University of Tennessee, Knoxville, TN 37996, USA
[3]SFP Works LLC, Washington, MI 48095, USA
†Corresponding author: Shassereba@ornl.gov

Key Words: Advanced High Strength Steels, Formability, Characterization

Notice of Copyright

This manuscript has been authored by UT-Battelle, LLC under Contract No. DE-AC05-00OR22725 with the U.S. Department of Energy. The United States Government retains and the publisher, by accepting the article for publication, acknowledges that the United States Government retains a non-exclusive, paid-up, irrevocable, world-wide license to publish or reproduce the published form of this manuscript, or allow others to do so, for United States Government purposes. The Department of Energy will provide public access to these results of federally sponsored research in accordance with the DOE Public Access Plan (http://energy.gov/downloads/doe-public-access-plan).

1. Abstract:

Flash processing is promising in making formable steel from economical low alloy steel. Flash processing involves a rapid heating and cooling cycle with short hold times. Different sections of a low alloy steel sheet, AISI 1023, was flash processed to four different peak temperatures. A spherical biaxial dome test measured the formability of the steel. After peak temperatures of 1170 ºC and 1270 ºC, the steel formed, showing loads and displacements comparable to those of expensive martensitic steel grades. The microstructures were characterized to correlate the processing with the observed formability. A martensitic microstructure was observed, with an average hardness of 510 HVN. Although the distribution of the values of hardness were 100 HVN. A hardness band, 20 to 30 HVN harder, was observed near the centerline in the steel exposed to the highest peak temperature. The hardness heterogeneity and distribution has been correlated to the measured formability of the steel.

2. Introduction:

The fuel economy of passenger vehicles can be increased by approximately 1.15% for every 10 kg of vehicle weight eliminated[1]. Advanced High-Strength Steels (AHSS) are among the materials being investigated for automotive use for this reason. AHSS have high tensile strength despite relatively low alloying content, which helps keep production costs low. Within the AHSS family, there are steels of various grades, including Quench and Partition (Q/P), Transformation Induced Plasticity (TRIP), Twinning-Induced Plasticity (TWIP), Dual Phase (DP), and Complex Microstructures (CP) [2-7]. These AHSS's obtain their strength and formability through unique processing routes, which produce complex microstructures. Steel microstructure, composed of hard and soft phase constituents, provides strength and ductility required for passenger/vehicle safety[8]. The microstructures can be a mix of ferrite and martensite (DP) [9], austenite and martensite (Q/P, TRIP, or TWIP) [10-12], or bainite and martensite (CP) [13]. The soft ferrite or austenite constituents provide ductility, and the hard martensite provides strength.

Recently, a new thermal processing technique, referred to as flash processing (FP) was developed. FP can produce strong, formable sheets of high-performance steel by incorporating fast heating rates (400ºC/s) and ultra-fast cooling rates (4000ºC/s) over short cycle times (<10 sec) [14, 15]. In FP, induction coils are used to rapidly heat the steel sheets. The heated sheets are then quenched with water. This process can produce a unique hardness distribution due to a complex microstructure of bainite and martensite in AISI 4130 [16, 17] and AISI 8620 [14] steels. This mixture of hard martensite and soft bainite microconstituents has been shown to provide strength and formability in traditional AHSS grades. In this study, AISI 1023 steel, a low carbon, generic, economical grade of steel, was flash processed in an attempt to generate the heterogenous microstructures seen in the flash processing of AISI 4130 and AISI 8620. The study measures the formability using a spherical punch dome test and presents the microstructure and inhomogeneous hardness distributions as it relates to formability.

3. Methods:

One sheet of AISI 1023 was obtained[1]for FP processing. The nominal composition of the sheet was 0.23C, 0.39Mn, 0.006P, 0.007S, 0.01Ni, 0.03Cr, 0.038Al, 0.03Cu (in wt%). The dimensions of the sheet were 610 mm X 3050 mm X 1.25 mm. One sheet of a commercially available 1500 MPa UTS steel sheet (1500MPa) sheet was obtained as a control[2]. The dimensions of the 1500MPa sheet were 610 mm X 304.8 mm X 1.25 mm.

3.1 Flash Processing

The FP was performed using a custom-built machine; a schematic of the machine is available in a study reported by Lola et al. (2014) [14]. The machine was equipped with top rollers to guide the sheets into the induction coil[3]. The coil was modified with custom magnetic-flux intensifiers. After passing through the magnetic flux intensifier field the sheets continued into a quenching bath. The sheet feed rate was 28 cm • min^{-1}. The temperature was monitored with an infrared pyrometer in the center of the 610 mm wide sheet[4]. Four flash temperatures were selected for testing: 1070ºC, 1140ºC, 1170ºC, and 1270ºC. The hold time at peak temperature was set to 2 seconds before quenching. The quenching bath was positioned 10 cm below the induction coils. Water jets within the bath forced water flow onto the steel sheets on both sides. The steel sheets emerged from the water bath through a rubber gasket guided by bottom-feed rollers.

3.2 Biaxial Dome Testing

Three disks, each 138.5 mm in diameter were cut from across the width at each temperature region, using a water jet. A custom-built “spherical punch” fixture was used to conduct formability testing (Figure 1a). The holder used bolts torqued to 122 N-m, that prevented slipping by clamping the disks at the perimeter. Figure 1b shows a CAD model of the disk holder. A high stress lubricant[5] was applied to the top of the steel sphere. A 500 kN MTS load frame configured for compression provided controlled punch displacement during testing. A 445

[1] Admiral Steel LLC., http://www.admiralsteel.com/, 4152 123rd St, Alsip, IL 60803
[2] AccelorMittal, http://www.usa.arcelormittal.com/
[3] Fluxtrol Inc., https://fluxtrol.com/, 1388 Atlantic Blvd, Auburn Hills, MI 48326
[4] Ircon, Fluke Process Instruments, http://www.ircon.com.cn/Ircon/en-r0
[5] Consultant Lubricants, Inc., http://www.clisyntec.com/index.html, 9 Research Park Drive St. Charles, MO 63304

kN load transducer[6] measured the load. The ram travel speed was set at 1.27 mm per sec. LabVIEW software recorded the load and dome displacement.

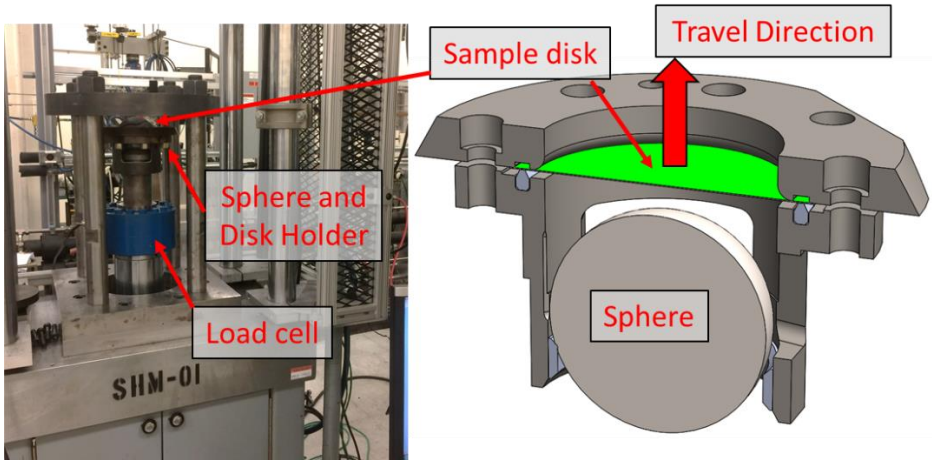

Figure 1. a) Image of test fixture, the disk holder and sphere loaded on top of the load cell. The fixture consisted of a large steel plate sitting on top of four posts. The large steel plate contained a hole in the middle, so the domes could form upward. A custom-built holder was used to hold a 100 mm steel sphere and the sample disks. b) Section drawing of disk holder with sphere.

3.3 Microstructural Analysis

Samples cut from the sheet near the disks were removed and were further sectioned using a silicon carbide wafer saw[7]. These samples were mounted in conductive phenolic resin. The samples were polished using standard metallographic techniques. The final polishing step was accomplished with 0.05 µm colloidal silica. An automatic microhardness tester[8] was used to map the through thickness hardness distribution on the polished cross sections. Electron Back Scatter Diffraction (EBSD) was conducted using Scanning Electron Microscopy (SEM) on a JEOL 6500 FEG-SEM at 20kV equipped with EDAX EBSD detector.

4. Results and Discussion:

4.1 Biaxial Dome Testing Results

The load versus dome displacement curves are shown in Figure 2. The disks flashed at 1070ºC and 1140ºC cracked along the circumference when tightening the bolts of the disk holder. The cracking almost traversed the entire circumference (~ 60%-75%). The clamping apparatus had to use aggressive clamping ring because the material would slip. The clamping ring had sharp radii which caused the cracking in these samples. During the test the circumferential cracks led to premature failure. One sample from each of the 1170ºC and 1270ºC regions taken from the middle of the 610 mm width, maintained integrity in the disk holder and gave a successful result (i.e., no slipping in the disk holder and no cracking due to clamping). The failure location for both disks was at the apex of the dome. However, the disks extracted on the side of the sheet, from these temperature locations, cracked when tightening the bolts. The results from the

[6] Interface Force Measurement Solutions, http://www.interfaceforce.com/, 7401 East Butherus Drive • Scottsdale, Arizona 85260
[7] Allied High Tech, http://www.alliedhightech.com/, 2376 East Pacifica Place Rancho Dominguez, CA 90220
[8] Leco, https://www.leco.com/

commercially available 1500MPa steel used for control, are included for comparison. The results show slightly higher dome displacement and load, from the 1500MPa. A forming limit diagram (FLD) from previous work is shown in Figure 2b [18]. The most right-hand side of the FLD represents data from the biaxial loading condition. The results from the current test align with the FLD comparing FP and a 1500 MPa martensitic steel.

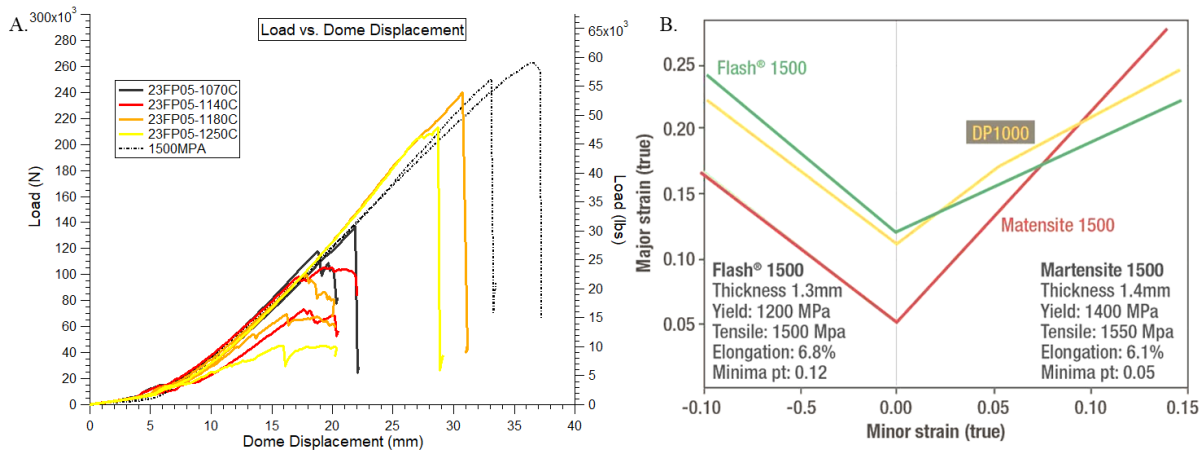

Figure 2. A. Load versus dome displacement of the 1023 steel sheet with varying flash temperatures. The curves for 1500MPa have been added for comparison. B. Forming limit diagram comparing FP 1020 steel (Flash 1500), DP1000, and Martensite 1500.(B. is from [18])

4.3 Pre-Flash Processing Microstructure

The microstructure prior to FP provides an important starting point for the final microstructure and related formability. The pre-FP microstructure showed spheroidal carbides indicative of a spheroidized condition, see Figure 3 for EBSD maps. In Figure 3a, the inverse pole figure orientations are superimposed on the image quality map, showing that the texture of the sheet was relatively random. In Figure 4b, the image quality map provides a good representation of the microstructure without the need for chemical etching. Here, the software applies a number on the greyscale to each pixel, which corresponds to an individual Kikuchi pattern. Then the software creates an image quality map of the greyscale pixels. The lighter grayscales represent higher quality Kikuchi patterns, whereas darker greyscales represent lower quality patterns (generally grain boundaries and carbides). Representative carbides/black dots are indicated by the black arrows in Figure 3b. The average ferrite grain size and carbide size are 7 µm and 1-2 µm, respectively.

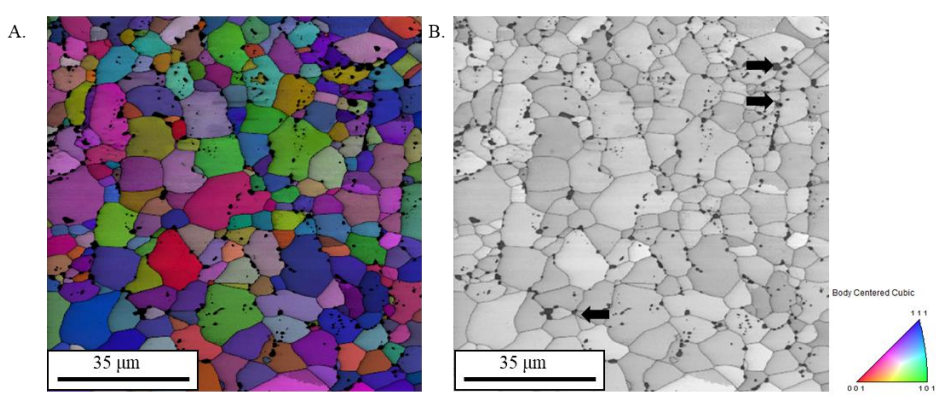

Figure 3. EBSD of As-Received material. A) Inverse pole figure map superimposed on the image quality map. B) Image quality map alone, spheroidized carbides are visible, as shown by black arrows.

4.4 Post Flash Processing Microstructure

The quenching step in FP produced a martensitic microstructure. The EBSD maps from samples with three different FP peak temperatures, increasing in 100ºC increments, are shown in Figure 4. In all conditions a fully martensitic microstructure was observed. No carbides were observed in the microstructure, suggesting that all the carbides dissolved during processing and the carbon redistributed in the austenite phase field. The prior austenite grain (PAG) size increased with increasing temperature, (see Fig. 4), which was expected [19, 20]. The PAG size has a direct relationship with the block and lath size of martensite, which then influences the strength and ductility of martensite [20-24]. This result would suggest that larger PAG sizes provide the formability in FP products. However, other modern AHSSs are also formable while maintaining a small PAG size [8, 9, 10-12, 13].

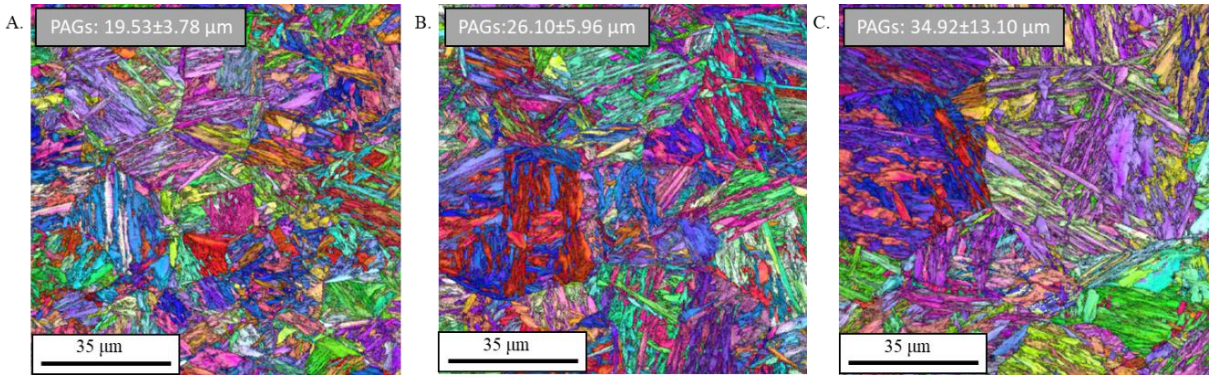

Figure 4. Inverse pole figure orientations superimposed onto image quality maps of FP 1023 steel A) 1070ºC, B) 1170ºC, C) 1270ºC. The PAG size is superimposed on the respective EBSD maps.

4.5 Hardness Mapping

The hardness profiles of the through thickness show a heterogenous hardness distribution. Figure 5 depicts the hardness profile, transverse to the rolling direction, from three different temperatures at 100ºC intervals. At the lowest peak temperature, there is some soft and hard heterogeneity. The average hardness of the lowest peak temperature sample is approximately 500 HVN. However, there is a wide deviation, roughly 125 HVN (Figure 6), of hardness values. The same features are also observed in the hardness profile from the 1170ºC sample. The average hardness is approximately 500 HVN and the deviation is also 125 HVN. The 1270ºC sample also shows a distribution of hard and soft regions, but an obvious hardness band is observed in the center of the sheet.

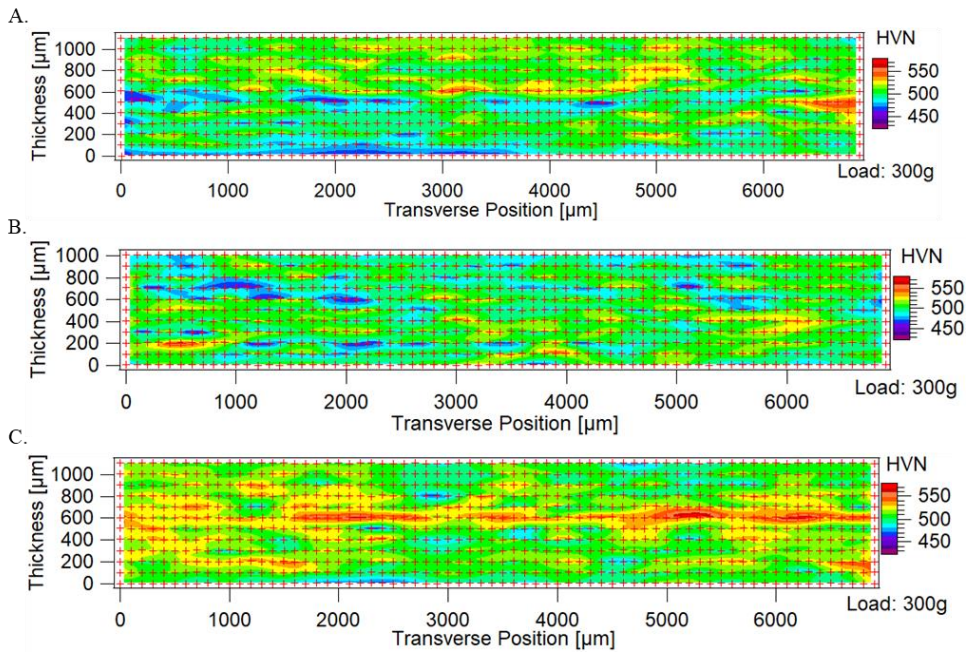

Figure 5. The hardness profiles for 1023 steel sheet cross sections at various flash temperatures A. 1070 ºC, B. 1170 ºC, and C. 1270 ºC. Rolling direction is out of the plane.

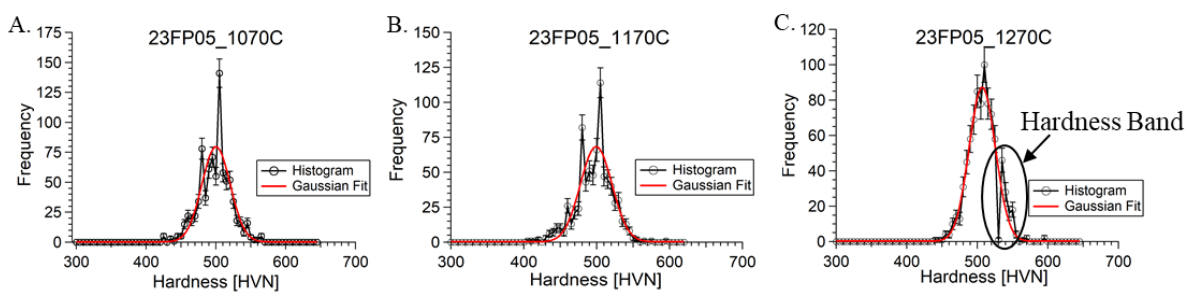

Figure 6. The histograms of the hardness from Figure 2 for A. 1070ºC, B. 1170ºC, and C. 1270ºC.

5. Summary:

FP utilizes a rapid heating and cooling cycle that can produce a strong and formable product from common low alloy, low carbon steel. The combination of the unique properties attained from the FP can add value to many industries, especially the automotive industry. The product can provide benefits in vehicle light-weighting and save on overall cost of vehicle manufacturing. In this study, the FP of 1023 steel has provided some insights on processing conditions and correlated microstructure to produce a formable sheet. There are still some aspects of FP that are yet to be understood. Research is continuing to understand the mechanism which provides the heterogenous microstructure and formability at high processing temperatures. A summary of results is listed below:

1. Further research is needed to correlate the processing to microstructure and properties
2. The PAG size increases with increasing FP temperature from 19 to 35μm.
3. Biaxial load displacement results of the 1170ºC and 1270°C FP sheet was nearly equivalent to a commercially purchased 1500MPa steel.
4. The through thickness hardness profile shows a unique heterogenous structure. At 1270 °C a centerline hardness band is observed.

6. Acknowledgements:

The authors thank Drs. Adrian Sabau and Chad Parish at Oak Ridge National Laboratory for their comments on this manuscript. This research is sponsored by the US Department of Energy, Advanced Manufacturing Office, under Contract DE-AC05-00OR22725 with UT-Battelle, LLC.

7. References:

[1] T. Senuma, Physical metallurgy of modern high strength steel sheets, Isij Int 41(6) (2001) 520-532.
[2] D.K. Matlock, J.G. Speer, E. De Moor, P.J. Gibbs, Recent developments in advanced high strength sheet steels for automotive applications: an overview, Jestech 15(1) (2012) 1-12.
[3] R. Kuziak, R. Kawalla, S. Waengler, Advanced high strength steels for automotive industry, Archives of civil and mechanical engineering 8(2) (2008) 103-117.
[4] O. Kwon, K.Y. Lee, G.S. Kim, K.G. Chin, New trends in advanced high strength steel developments for automotive application, Materials Science Forum, Trans Tech Publ, 2010, pp. 136-141.
[5] M. Takahashi, Development of high strength steels for automobiles, Shinnittetsu Giho (2003) 2-6.
[6] G. Jha, S. Das, S. Sinha, A. Lodh, A. Haldar, Design and development of precipitate strengthened advanced high strength steel for automotive application, Materials Science and Engineering: A 561 (2013) 394-402.
[7] D. Raabe, D. Ponge, O. Dmitrieva, B. Sander, Designing ultrahigh strength steels with good ductility by combining transformation induced plasticity and martensite aging, Advanced Engineering Materials 11(7) (2009) 547-555.
[8] L.A. Kestens, D. De Knijf, F.C. Cerda, R.H. Petrov, Advanced High Strength Steels: Improved Properties by Design of Textures and Microstructures, IOP Conf. Series: Mater. Sci. Eng, 2017.
[9] M. Sarwar, R. Priestner, Influence of ferrite-martensite microstructural morphology on tensile properties of dual-phase steel, Journal of Materials Science 31(8) (1996) 2091-2095.
[10] B.C. De Cooman, J.G. Speer, Quench and Partitioning Steel: A New AHSS Concept for Automotive Anti-Intrusion Applications, steel research international 77(9-10) (2006) 634-640.
[11] S. Zaefferer, J. Ohlert, W. Bleck, A study of microstructure, transformation mechanisms and correlation between microstructure and mechanical properties of a low alloyed TRIP steel, Acta Materialia 52(9) (2004) 2765-2778.
[12] D. Barbier, N. Gey, S. Allain, N. Bozzolo, M. Humbert, Analysis of the tensile behavior of a TWIP steel based on the texture and microstructure evolutions, Materials Science and Engineering: A 500(1) (2009) 196-206.
[13] J.P. Naylor, Influence of the Lath Morphology on the Yield Stress and Transition-Temperature of Martensitic-Bainitic Steels, Metall Trans A 10(7) (1979) 861-873.

[14] T. Lolla, G. Cola, B. Narayanan, B. Alexandrov, S.S. Babu, Development of rapid heating and cooling (flash processing) process to produce advanced high strength steel microstructures, Materials Science and Technology 27(5) (2013) 863-875.
[15] D.J. Tung, T. Lolla, S. Babu, G. Cola, FLASH PROCESSING PRODUCES UNIQUE COMBINATION OF PROPERTIES IN STEELS, ADVANCED MATERIALS & PROCESSES (2013).
[16] B. Hanhold, S.S. Babu, G. Cola, Investigation of heat affected zone softening in armour steels Part 1 – Phase transformation kinetics, Science and Technology of Welding and Joining 18(3) (2013) 247-252.
[17] B. Hanhold, S.S. Babu, G. Cola, Investigation of heat affected zone softening in armour steels Part 2 – Mechanical and microstructure heterogeneity, Science and Technology of Welding and Joining 18(3) (2013) 253-260.
[18] D.R. Forrest, T. Miller, S.S. Babu, B. Shassere, G. Cola, Flash® Processing for High-Strength, Cold-Stampable Automotive Steel, Industrial Heating (2017).
[19] S. Morito, H. Tanaka, R. Konishi, T. Furuhara, T. Maki, The morphology and crystallography of lath martensite in Fe-C alloys, Acta Materialia 51(6) (2003) 1789-1799.
[20] S. Morito, H. Yoshida, T. Maki, X. Huang, Effect of block size on the strength of lath martensite in low carbon steels, Materials Science and Engineering: A 438-440 (2006) 237-240.
[21] H.K.D.H. Bhadeshia, Martensite in Steels, (2002).
[22] H. Kitahara, R. Ueji, N. Tsuji, Y. Minamino, Crystallographic features of lath martensite in low-carbon steel, Acta Materialia 54(5) (2006) 1279-1288.
[23] S. Morito, T. Ohba, T. Maki, Comparison of Deformation Structure of Lath Martensite in Low Carbon and Ultra-Low Carbon Steels, Materials Science Forum 558-559 (2007) 933-938.
[24] A. Shibata, T. Nagoshi, M. Sone, S. Morito, Y. Higo, Evaluation of the block boundary and sub-block boundary strengths of ferrous lath martensite using a micro-bending test, Mat Sci Eng a-Struct 527(29-30) (2010) 7538-7544.